Research Square

Preprints are preliminary reports that have not undergone peer review.
They should not be considered conclusive, used to inform clinical practice,
or referenced by the media as validated information.

Spatial Growth Optimization with Mechanical Boundary Constraints and Active Dissipation

Robert Vrabel

robert.vrabel@stuba.sk

Slovak University of Technology in Bratislava, Jana Bottu 25

Research Article

Keywords: Growth, Mechanics, Transversality, Riccati control, Dissipation, Mass supply

Posted Date: November 23rd, 2026

DOI: https://doi.org/10.21203/rs.3.rs-11773059/v1

License: This work is licensed under a Creative Commons Attribution 4.0 International License.
Read Full License

Additional Declarations: No competing interests reported.

Spatial Growth Optimization with Mechanical Boundary Constraints and Active Dissipation

Robert Vrabel[1*]

[1*]Institute of Applied Informatics, Automation and Mechatronics, Slovak University of Technology in Bratislava, Jana Bottu 25, 917 01 Trnava, Slovakia.

Corresponding author(s). E-mail(s): robert.vrabel@stuba.sk;

Abstract

Spatial growth optimization couples mechanical boundary conditions with thermodynamic restrictions associated with material deposition. We develop an optimal-control formulation incorporating mixed terminal constraints, Riccati-based propagation of terminal multipliers and a local open-system dissipation inequality enforced through a distributed multiplier. For a spherical shell, radial equilibrium and incremental compatibility furnish a spatial state system. Exact analytical solutions demonstrate the role of terminal mechanical constraints and quantify the boundary-condition violation produced by free-endpoint optimality conditions. A coupled two-state benchmark extends this result to unequal incremental moduli. The thermodynamic formulation accounts explicitly for the specific free energy carried by supplied material. For a prescribed affine reduced-dissipation model, we derive an exact activation threshold, construct the optimal solution with an active dissipation constraint and determine its switching location. A nonnegative distributed multiplier and a direct cost-difference identity establish global optimality and uniqueness. Exact cellwise state propagation provides an independent numerical verification. The resulting framework combines mechanical boundary constraints and thermodynamic admissibility within spatial growth optimization.

Keywords: Growth, Mechanics, Transversality, Riccati control, Dissipation, Mass supply

MSC 2020 Classification: 49K15 , 49N10 , 74A15 , 74F25

1 Introduction

Growth and remodelling change the mass content, geometry and residual stress of a solid. Deposition and removal of material interact with mechanical loading, while growth in one region can be coordinated with conditions elsewhere in the body. Models of finite growth and remodelling therefore include evolving material configurations, residual and configurational stresses, constitutive evolution laws and transport of mass and energy. Central developments include the thermomechanics of volumetric growth [1], constrained mixtures [2], continuum mass transport and tissue growth [3], finite-growth kinematics and constitutive formulations [4–6], and more recent mechanobiological and analytical-mechanics descriptions [7–10]. These theories provide the mechanical and thermodynamic setting in which spatially distributed growth is to be optimized.

Growth has also been studied as a control process: bone adaptation has been formulated as an optimal-control problem [11, 12], prescribed incompatible strains have been optimized to produce target plate shapes [13], and artery growth laws have been constructed using reinforcement learning [14]. A spatial optimal-control formulation uses a material coordinate as its independent variable, with equilibrium and compatibility represented by evolution equations along that coordinate. For a radial shell, equilibrium and compatibility become a first-order system in the reference radius. The control specifies part of the incremental mechanical field, while the state records the associated stress and growth-rate profiles.

This spatial reformulation creates a structural requirement that has no analogue in an unconstrained terminal regulator: the terminal point of the spatial trajectory is an actual material boundary. Traction or displacement data therefore define a terminal set, and the corresponding endpoint variations are constrained. The second law supplies another, independent restriction: deposition changes mass content, and the incoming material carries an energy supply that determines which growth increments are admissible. A viable spatial optimum must satisfy both restrictions *during* the optimization, not merely when the result is checked afterwards.

Recent spatial growth-control models, including the radial shell formulation of Huang [15] and its constitutive background in Huang et al. [16], provide a useful setting for identifying terminal traction constraints and source-dependent dissipation in spatial optimization. In a shell with one prescribed radial-stress component and one free terminal component, the mechanical boundary data define a mixed terminal manifold.

The principal contributions of this work are threefold. First, we develop an endpoint-constrained Riccati formulation with propagated terminal multipliers and demonstrate its mechanical significance through exact spherical-shell solutions, including a coupled two-state benchmark with unequal incremental moduli. Second, we establish an open-system dissipation formulation that explicitly accounts for the specific free energy supplied with deposited material and derive a constitutive compatibility criterion for reduced dissipation laws. Third, we incorporate the local dissipation inequality directly into spatial optimization and obtain an exact activation threshold, an analytical switching solution, and a direct certificate of global optimality and uniqueness. Classical terminal-constrained optimal control and open-system thermodynamics provide the theoretical foundations [17–20], while their integration with mechanical boundary conditions and local dissipation constraints yields explicit analytical benchmarks. Exact

cellwise state propagation provides independent numerical verification of the resulting optimal solutions.

The endpoint construction and its linear-quadratic realization are developed in Sections 2 and 3. Section 4 derives source-dependent dissipation, and Section 5 formulates the joint terminal/path-constrained problem. Section 6 derives the radial shell equations, gives two independent endpoint calculations, distinguishes constitutive coefficients from geometric source terms, and constructs an exactly certified active-dissipation solution. Section 7 examines the mechanical and thermodynamic implications of the resulting optimality conditions.

2 Spatial optimal control with a mechanically constrained terminal state

2.1 General spatial problem

Let $s \in [a, b]$ be a spatial parameter along a material curve, fibre, layer or another one-dimensional reduction of a continuum problem. Consider

$$y'(s) = f(y(s), u(s), s), \qquad y(a) = y_a, \tag{1}$$

where $y(s) \in \mathbb{R}^n$ and $u(s) \in \mathbb{R}^{n_u}$. Admissible controls are taken in $L^\infty([a, b]; \mathbb{R}^{n_u})$ and the corresponding states are absolutely continuous. The cost functional is

$$\mathcal{J}[u] = \Phi(y(b)) + \int_a^b \ell(y(s), u(s), s)\, ds. \tag{2}$$

Here $\Phi : \mathbb{R}^n \to \mathbb{R}$ is the terminal cost and $\ell : \mathbb{R}^n \times \mathbb{R}^{n_u} \times [a, b] \to \mathbb{R}$ is the scalar running-cost density. The terminal mechanical conditions are represented by

$$g(y(b)) = 0, \qquad g : \mathbb{R}^n \to \mathbb{R}^q, \qquad q \le n, \tag{3}$$

with $Dg(y_b)$ of full row rank at the terminal point $y_b = y(b)$. Thus the admissible terminal states lie on the smooth manifold

$$\mathcal{M}_b = \{y \in \mathbb{R}^n : \ g(y) = 0\}. \tag{4}$$

The spatial Hamiltonian is defined by

$$\mathcal{H}(y, u, p, s) = \ell(y, u, s) + p^T f(y, u, s). \tag{5}$$

The sign convention is chosen for a minimization problem.

Terminal-manifold Pontryagin conditions.
Assume that f, ℓ, Φ and g are continuously differentiable, that an optimal pair (y^*, u^*) exists with y^* absolutely continuous and $u^* \in L^\infty([a, b]; \mathbb{R}^{n_u})$, and that $Dg(y^*(b))$ has

full row rank. Suppose that the extremal is normal, with the cost multiplier normalized to one, and that the control set is $U = \mathbb{R}^{n_u}$ with $u^*(s)$ an interior control for almost every s. Then there exist an absolutely continuous costate $p : [a, b] \to \mathbb{R}^n$ and a multiplier $\lambda \in \mathbb{R}^q$ such that

$$y^{*\prime} = \frac{\partial \mathcal{H}}{\partial p}(y^*, u^*, p, s), \tag{6}$$

$$p' = -\frac{\partial \mathcal{H}}{\partial y}(y^*, u^*, p, s), \tag{7}$$

with the stationarity condition

$$\frac{\partial \mathcal{H}}{\partial u}(y^*, u^*, p, s) = 0 \tag{8}$$

for an unconstrained interior control, and the terminal transversality condition

$$p(b) = \nabla \Phi(y^*(b)) + Dg(y^*(b))^T \lambda. \tag{9}$$

Equivalently,

$$\big[p(b) - \nabla \Phi(y^*(b))\big]^T \delta y_b = 0 \tag{10}$$

for every terminal variation $\delta y_b \in T_{y^*(b)}\mathcal{M}_b$, where $T_{y^*(b)}\mathcal{M}_b = \ker Dg(y^*(b))$ denotes the tangent space to $\mathcal{M}_b$ at $y^*(b)$.

To obtain these conditions, introduce the augmented functional

$$\mathcal{J}_a = \Phi(y(b)) + \lambda^T g(y(b)) + \int_a^b \big[\ell(y, u, s) + p^T (f(y, u, s) - y')\big] ds. \tag{11}$$

Integration by parts of the term $-p^T \delta y'$ gives

$$\begin{aligned} \delta \mathcal{J}_a = {} & \big[\nabla \Phi(y(b)) + Dg(y(b))^T \lambda - p(b)\big]^T \delta y(b) \\ & + p(a)^T \delta y(a) \\ & + \int_a^b \Big[\big(\ell_y + f_y^T p + p'\big)^T \delta y \\ & \qquad + \big(\ell_u + f_u^T p\big)^T \delta u \Big] ds. \end{aligned} \tag{12}$$

Because $y(a) = y_a$ is fixed, $\delta y(a) = 0$. Vanishing of the integral terms gives (7) and (8), while the terminal term gives (9). The tangent-space form (10) follows because $Dg(y_b)\delta y_b = 0$ for admissible terminal variations.

The mechanical interpretation of (9) is direct: the terminal manifold is determined by prescribed boundary data, while its normal multiplier transmits those data into the adjoint system. Mixed terminal conditions are therefore intrinsic to spatial control of stress and deformation fields.

Mixed fixed/free terminal components.
Let $y = (y_c, y_f)$ with

$$y_c(b) = \bar{y}_c, \qquad y_f(b) \text{ free}, \tag{13}$$

where $y_c \in \mathbb{R}^q$ and $y_f \in \mathbb{R}^{n-q}$. Then the transversality conditions are

$$p_f(b) = \frac{\partial \Phi}{\partial y_f}(y(b)), \tag{14}$$

whereas $p_c(b)$ is not prescribed by the terminal cost. It is determined together with the multiplier associated with $y_c(b) = \bar{y}_c$.

Equation (14) is the useful practical rule. A prescribed terminal state component has zero admissible variation, so no transversality equation is generated for its conjugate costate. Applying the free-endpoint condition to that component introduces an additional boundary condition which is not part of the variational problem.

3 Linear-quadratic specialization and endpoint-constrained Riccati theory

The general endpoint result is now specialized to a linear-quadratic structure. This step is useful because precisely such a structure arises in the radial-fibre shell model discussed in Section 6, and it permits a Riccati-based computational realization of the terminal-manifold condition.

3.1 Linear-quadratic spatial regulator

Consider

$$y' = A(s)y + B(s)u, \qquad y(a) = y_a, \tag{15}$$

with the quadratic functional

$$\mathcal{J} = \frac{1}{2}(y(b) - r_b)^T H (y(b) - r_b) + \frac{1}{2}\int_a^b \left[(y - r)^T Q (y - r) + (u - u_0)^T R (u - u_0)\right] ds, \tag{16}$$

where $H = H^T \geq 0$, $Q = Q^T \geq 0$, the coefficient functions are continuous, and $R = R^T$ is uniformly positive definite on $[a, b]$, i.e. $R(s) \geq r_0 I$ for some $r_0 > 0$. Let the terminal mechanical condition be affine,

$$Cy(b) = d, \qquad C \in \mathbb{R}^{q \times n}, \qquad \operatorname{rank} C = q. \tag{17}$$

The Hamiltonian is

$$\mathcal{H} = \frac{1}{2}(y - r)^T Q (y - r) + \frac{1}{2}(u - u_0)^T R (u - u_0) + p^T (Ay + Bu). \tag{18}$$

The first-order conditions are

$$y' = Ay + Bu, \tag{19}$$

$$p' = -A^T p - Q(y - r), \tag{20}$$
$$u = u_0 - R^{-1} B^T p, \tag{21}$$

and the terminal condition is

$$p(b) = H(y(b) - r_b) + C^T \lambda. \tag{22}$$

Finite-horizon linear-quadratic problems with affine boundary constraints admit established optimal-control formulations [17, 18]. The differential-Riccati realization used here is particularly suitable for the spatially varying growth coefficients. The affine ansatz $p = Ky + z$ is augmented by a propagated terminal multiplier so that the mechanical boundary condition is satisfied without sacrificing the Riccati structure.

Endpoint-constrained Riccati representation.

Assume that the linear-quadratic problem (15)–(17) is feasible and normal, that the terminal-value problems below admit solutions on $[a, b]$, and that the terminal sensitivity matrix $CY(b)$ defined in (32) has full rank q. Let

$$p(s) = K(s)y(s) + z(s) + Z(s)\lambda, \tag{23}$$

where $K \in \mathbb{R}^{n\times n}$, $z \in \mathbb{R}^n$ and $Z \in \mathbb{R}^{n\times q}$. Then the state–costate system (19)–(22) is represented by

$$K' + KA + A^T K - KBR^{-1}B^T K + Q = 0, \tag{24}$$
$$z' + \left(A - BR^{-1}B^T K\right)^T z - Qr + KBu_0 = 0, \tag{25}$$
$$Z' + \left(A - BR^{-1}B^T K\right)^T Z = 0, \tag{26}$$

with terminal data

$$K(b) = H, \qquad z(b) = -Hr_b, \qquad Z(b) = C^T. \tag{27}$$

Moreover $K(s) = K(s)^T$ on its interval of existence, the optimal control is

$$u = u_0 - R^{-1}B^T(Ky + z + Z\lambda), \tag{28}$$

and the full-rank sensitivity condition yields a unique terminal multiplier λ through (34).

The representation follows directly from the state–costate equations. Because H and Q are symmetric, the Riccati equation with $K(b) = H$ preserves symmetry, hence $K^T = K$. Substitution of (23) into (21) gives

$$y' = A_c y + Bu_0 - BR^{-1}B^T z - BR^{-1}B^T Z\lambda, \qquad A_c = A - BR^{-1}B^T K. \tag{29}$$

Differentiating (23) and using (20) and (29), the coefficient of y gives (24), the multiplier-independent affine part gives (25), and the coefficient of the constant vector λ gives (26). The terminal data yield

$$p(b) = Hy(b) - Hr_b + C^T\lambda,$$

which is exactly (22). Finally, the decomposition $y = \bar{y} + Y\lambda$ gives (34); the assumed full rank of the square matrix $CY(b) \in \mathbb{R}^{q\times q}$ makes the multiplier unique.

Because the dynamics and endpoint constraint are affine and the cost functional is convex, with a uniformly positive-definite control weight, the above first-order conditions are also sufficient. Consequently, every feasible extremal satisfying (24)–(34) is the global minimizer, and the optimal control is unique.

For computation, the terminal multiplier can be extracted from one additional forward sensitivity system. Let

$$y = \bar{y} + Y\lambda, \tag{30}$$

where $\bar{y}$ solves

$$\bar{y}' = A_c\bar{y} + Bu_0 - BR^{-1}B^Tz, \qquad \bar{y}(a) = y_a, \tag{31}$$

and

$$Y' = A_cY - BR^{-1}B^TZ, \qquad Y(a) = 0, \tag{32}$$

with

$$A_c = A - BR^{-1}B^TK. \tag{33}$$

Then

$$CY(b)\lambda = d - C\bar{y}(b). \tag{34}$$

Under the full-rank assumption stated above, $CY(b)$ is nonsingular and

$$\lambda = [CY(b)]^{-1}[d - C\bar{y}(b)]. \tag{35}$$

For $q < n$, only a $q \times q$ linear system must be solved after the backward Riccati integration and the forward state/sensitivity integration.

Exact condition for a vanishing terminal multiplier.

Under the same assumptions,

$$\lambda = 0 \quad \Longleftrightarrow \quad C\bar{y}(b) = d. \tag{36}$$

Thus the standard affine Riccati trajectory $p = Ky + z$ is mechanically admissible without a multiplier term if and only if its associated free-endpoint trajectory already lands on the prescribed terminal manifold. Otherwise the terminal multiplier is necessarily nonzero. This equivalence follows immediately from (35) and the nonsingularity of $CY(b)$.

Free terminal vector as a special case.

If $q = 0$, there is no terminal mechanical constraint, Z disappears and the representation reduces to the classical conditions

$$K(b) = H, \qquad z(b) = -Hr_b, \tag{37}$$

which imply $p(b) = H(y(b) - r_b)$. If $q > 0$, the same two terminal conditions for K and z remain useful, but they are not sufficient by themselves: the additional term $Z\lambda$ is essential unless the terminal multiplier happens to vanish.

A minimal algebraic example illustrating why the fully free terminal condition is incompatible with a prescribed terminal state is given in Appendix A. The following sections focus on how these endpoint conditions interact with mass production and radial mechanics.

4 Open-system Clausius–Duhem inequality for growth

We consider a single-constituent solid with a local volumetric mass source, no relative mass flux, and no independent momentum or relative kinetic-energy supply from the deposited material. Deposited mass joins the continuum at the local velocity; the energetic and entropic source quantities are evaluated at the local temperature under local equilibrium. These assumptions specify the balance structure needed for the radial growth model, using standard continuum stress-power and thermodynamic conventions [21]. More general open-system balances include relative mass transport and corresponding momentum and entropy fluxes [3, 20].

4.1 Mass balance with production

Let $\mathcal{B}_t$ be the current configuration, with density ρ, velocity v, deformation gradient F, Jacobian $J = \det F > 0$ and velocity gradient $L = \dot{F}F^{-1}$. Let

$$D = \frac{1}{2}(L + L^T). \tag{38}$$

Growth with mass production is described locally by

$$\dot{\rho} + \rho \operatorname{tr} L = \Gamma, \tag{39}$$

where Γ is the local mass supply per unit current volume and unit time. The referential density is

$$\rho_0 = J\rho. \tag{40}$$

Since $\dot{J} = J \operatorname{tr} L$, Eq. (39) gives

$$\dot{\rho}_0 = J\Gamma =: M, \tag{41}$$

where M is the mass supply per unit reference volume.

Equation (41) makes one point immediate: a model with $\dot{\rho}_0 \neq 0$ is an open-system model even if the reference configuration itself is fixed.

4.2 Energy and entropy balances with supplied mass

Let e and η be the specific internal energy and entropy, θ the absolute temperature, q the heat flux, r_h the heat supply per unit mass, and σ the Cauchy stress. Let the supplied mass carry specific internal energy e_s and specific entropy η_s, both evaluated at the local temperature under the convention stated above. For a material control volume moving with the velocity v, the local energy balance is

$$\rho \dot{e} = \sigma : D - \operatorname{div} q + \rho r_h + \Gamma(e_s - e). \tag{42}$$

The corresponding entropy inequality is

$$\rho \dot{\eta} + \Gamma \eta \geq \frac{\rho r_h}{\theta} - \operatorname{div}\left(\frac{q}{\theta}\right) + \Gamma \eta_s. \tag{43}$$

The terms $-\Gamma e$ and $-\Gamma \eta$ on the local left-hand side are not additional constitutive assumptions. They arise automatically because the time derivative of an extensive quantity in a material volume contains the mass-production contribution.

Define the specific Helmholtz free energy

$$\psi = e - \theta \eta, \qquad \psi_s = e_s - \theta \eta_s. \tag{44}$$

Open-system Clausius–Duhem inequality.
The balances (39), (42) and (43) imply

$$\mathcal{D} = \sigma : D - \rho(\dot{\psi} + \eta \dot{\theta}) - \frac{1}{\theta} q \cdot \nabla \theta + \Gamma(\psi_s - \psi) \geq 0. \tag{45}$$

In an isothermal process with $\dot{\theta} = 0$ and $\nabla \theta = 0$,

$$\mathcal{D} = \sigma : D - \rho \dot{\psi} + \Gamma(\psi_s - \psi) \geq 0. \tag{46}$$

To derive (45), multiply (43) by θ and use

$$\theta \operatorname{div}\left(\frac{q}{\theta}\right) = \operatorname{div} q - \frac{1}{\theta} q \cdot \nabla \theta.$$

Eliminating $\rho r_h - \operatorname{div} q$ with the energy balance (42) gives

$$\sigma : D - \rho(\dot{e} - \theta \dot{\eta}) - \frac{1}{\theta} q \cdot \nabla \theta + \Gamma[(e_s - e) - \theta(\eta_s - \eta)] \geq 0.$$

Since $\dot{e} - \theta \dot{\eta} = \dot{\psi} + \eta \dot{\theta}$ and the bracketed source term equals $\psi_s - \psi$, Eq. (45) follows.

4.3 Reference-energy representation and the density-rate term

Let

$$\Psi_0 = \rho_0 \psi \tag{47}$$

be the free energy per unit reference volume and

$$P = J\sigma F^{-T} \tag{48}$$

the first Piola–Kirchhoff stress. In the isothermal case, multiply (46) by J and use

$$P : \dot{F} = J\sigma : L = J\sigma : D \tag{49}$$

for symmetric σ. Because

$$\dot{\Psi}_0 = \rho_0\dot{\psi} + \psi\dot{\rho}_0, \tag{50}$$

we obtain the referential form.

Referential open-system dissipation.

Under the assumptions stated above, the isothermal dissipation inequality is equivalently

$$\mathcal{D}_0 = P : \dot{F} - \dot{\Psi}_0 + \psi_s\dot{\rho}_0 \geq 0. \tag{51}$$

Indeed, using $M = J\Gamma = \dot{\rho}_0$,

$$\begin{aligned} J\mathcal{D} &= P : \dot{F} - \rho_0\dot{\psi} + \dot{\rho}_0(\psi_s - \psi) \\ &= P : \dot{F} - \dot{\Psi}_0 + \psi_s\dot{\rho}_0. \end{aligned}$$

Differentiation of $\Psi_0 = \rho_0\psi$ contributes $\psi\dot{\rho}_0$, which combines with the mass-supply term to give $\psi_s\dot{\rho}_0$ in (51). The reference and current formulations therefore identify the same source-energy contribution. Its algebraic representation depends on the free-energy density employed, while the supplied specific free energy determines the source contribution in either description.

Source-neutral closure.

If the supplied mass is assumed to carry the same specific free energy as the local material,

$$\psi_s = \psi, \tag{52}$$

then the current dissipation inequality reduces to

$$\mathcal{D} = \sigma : D - \rho\dot{\psi} \geq 0, \tag{53}$$

while its referential representation is

$$\mathcal{D}_0 = P : \dot{F} - \dot{\Psi}_0 + \psi\dot{\rho}_0 \geq 0. \tag{54}$$

Thus the closed-system-looking current form (53) is compatible with nonzero mass production, but only under the closure (52) or an energetically equivalent assumption.

Interpretation of the density-rate term.

The source-neutral relation (52) is a constitutive closure. In the specific-energy and intermediate-volume representations, mass-density derivatives are reorganized by the product rule, while the energetic state of the supplied material remains encoded by ψ_s. Broader open-system theories can incorporate additional mass fluxes, chemical potentials and configurational power; the scalar ψ_s describes the local-source setting considered here.

4.4 Intermediate unloaded configuration with constant density

A class of volumetric-growth models introduces an unloaded configuration $\bar{\mathcal{B}}$ with

$$F = F_e \bar{F}, \qquad J = J_e \bar{J}, \tag{55}$$

and assumes elastic incompressibility $J_e = 1$. Suppose additionally that the mass density $\bar{\rho}$ per unit volume of $\bar{\mathcal{B}}$ is constant during growth. Then

$$\rho_0 = \bar{\rho}\bar{J}, \qquad \rho = \bar{\rho}, \tag{56}$$

so that

$$\dot{\rho}_0 = \rho_0 \operatorname{tr} \bar{L}, \qquad \Gamma = \rho \operatorname{tr} \bar{L}, \qquad \bar{L} = \dot{\bar{F}}\bar{F}^{-1}. \tag{57}$$

Defining the free energy per unit volume of $\bar{\mathcal{B}}$ by

$$\bar{\Psi} = \bar{\rho}\psi, \tag{58}$$

we have $\dot{\bar{\Psi}} = \rho\dot{\psi}$. Hence (46) becomes

$$\mathcal{D} = \sigma : D - \dot{\bar{\Psi}} + \rho(\psi_s - \psi) \operatorname{tr} \bar{L} \geq 0. \tag{59}$$

The last term vanishes under the source-neutral closure but is otherwise part of the growth driving force. In tensor form,

$$\rho(\psi_s - \psi) \operatorname{tr} \bar{L} = \rho(\psi_s - \psi) I : \bar{L}. \tag{60}$$

Thus a non-neutral mass source shifts the thermodynamic force conjugate to the volumetric part of the growth-rate tensor by an isotropic contribution.

5 Thermodynamically admissible spatial optimal control

The preceding sections can be combined without identifying the control with a particular growth variable. Let y and u parameterize a spatial reduction of the incremental growth problem and suppose that the continuum constitutive equations induce a local dissipation function

$$\mathcal{D}_s = \mathcal{D}_s(y, u, s). \tag{61}$$

For an open-system growth process, $\mathcal{D}_s$ must include the appropriate source-energy term from Section 4. The admissible spatial optimal-control problem is

$$\min_u \ \Phi(y(b)) + \int_a^b \ell(y,u,s)\,ds \tag{62}$$

subject to

$$y' = f(y,u,s), \tag{63}$$
$$y(a) = y_a, \tag{64}$$
$$g(y(b)) = 0, \tag{65}$$
$$\mathcal{D}_s(y,u,s) \geq 0 \quad \text{a.e. on } [a,b]. \tag{66}$$

The endpoint constraint and the dissipation inequality act at different levels: the first determines the admissible terminal manifold, while the second restricts the control at every material radius. The resulting optimization couples a finite-dimensional terminal multiplier with a spatially distributed complementary multiplier. In a convex linear-quadratic reduction with an affine dissipation inequality, this combined structure admits global sufficiency: a feasible solution of the state, adjoint, stationarity, endpoint and complementarity equations is the unique minimizer whenever the control cost is strictly convex. Here $y : [a,b] \to \mathbb{R}^n$ is the spatial mechanical state, $u : [a,b] \to \mathbb{R}^{n_u}$ is the control, and $p : [a,b] \to \mathbb{R}^n$ is the adjoint or costate. We denote the multiplier of the terminal equality by $\lambda \in \mathbb{R}^q$ and the multiplier of the unilateral path constraint by $\mu : [a,b] \to [0,\infty)$. In particular, μ is *not* a costate; it acts only where dissipation reaches its limiting value. The scalar $\mathcal{D}_s$ is the local dissipation rate per current volume in the isothermal specialization, evaluated through the chosen constitutive closure and reduced growth variables. A nonnegative dissipation checked after optimization is not equivalent to enforcing the inequality during optimization.

Regular mixed dissipation constraint.

Assume that $\mathcal{D}_s(y,u,s)$ is continuously differentiable and is a regular mixed state-control constraint. More precisely, on the active set $\mathcal{D}_s(y^*,u^*,s) = 0$, assume a mixed-constraint qualification of Mangasarian–Fromowitz type; for the scalar constraint used here it is sufficient that there exists a control direction $d_u(s)$ such that

$$\frac{\partial \mathcal{D}_s}{\partial u}(y^*,u^*,s)d_u(s) > 0 \quad \text{a.e. on the active set.} \tag{67}$$

Assume in addition a normal extremal and an unconstrained ambient control set. Then there are a terminal multiplier $\lambda \in \mathbb{R}^q$ and a measurable multiplier $\mu(s) \geq 0$ such that the augmented Hamiltonian

$$\mathcal{H}_a = \ell + p^T f - \mu \mathcal{D}_s \tag{68}$$

satisfies

$$y' = \frac{\partial \mathcal{H}_a}{\partial p} = f, \tag{69}$$

$$p' = -\frac{\partial \mathcal{H}_a}{\partial y}, \tag{70}$$

$$0 = \frac{\partial \mathcal{H}_a}{\partial u}, \tag{71}$$

with

$$p(b) = \nabla\Phi(y(b)) + Dg(y(b))^T\lambda, \tag{72}$$

and

$$\mu \geq 0, \qquad \mathcal{D}_s \geq 0, \qquad \mu\mathcal{D}_s = 0 \quad \text{a.e.} \tag{73}$$

along the extremal.

These conditions are the smooth scalar specialization of standard maximum-principle results for regular mixed control-state constraints; see, for example, Clarke and de Pinho [22] and Boccia et al. [23]. Pure state path constraints generally require a different multiplier structure, potentially involving measures and additional junction conditions.

The multiplier μ has a direct computational interpretation. Where $\mathcal{D}_s > 0$, complementarity gives $\mu = 0$ and the state–costate system follows its unconstrained spatial optimum. Where $\mathcal{D}_s = 0$, the multiplier modifies the stationarity equation and hence the optimal control. The switching points between these regions are part of the solution. In Section 6.5 this structure becomes explicit: the active interval, control law and switching radius are computed, and positivity of the mixed-constraint multiplier yields an optimality certificate.

For an affine reduced constraint $\mathcal{D}_s = d_0(s) + d_y(s)^T y + d_u(s)^T u$, the scalar regularity condition is $d_u(s) \neq 0$ on the active set. If an effective control coefficient vanishes, the inequality may become a pure-state condition and a different maximum-principle multiplier structure is needed. Spatially variable constitutive coefficients may also produce several disjoint active intervals. The exact-cell quadratic-programming approach employed below does not prescribe their number in advance; the one-switch formula is a property of the particular benchmark, established by its optimality certificate.

A posteriori checking versus constrained optimization.

If the dissipation inequality is checked only after solving an unconstrained optimal-control problem, the result may fail to be thermodynamically admissible even when the unconstrained optimum is mathematically correct. The multiplier formulation (68)–(73) provides a systematic alternative whenever the dissipation condition is intended to be enforced a priori.

6 Radial shell mechanics and explicit constrained-control benchmarks

6.1 Mechanical variables, equilibrium and compatibility

Consider a spherical solid shell with fixed reference radii $R_i < R_o$. Let R denote the reference material radius and $\bar{r}(R)$ the radius in an intermediate, elastically unloaded configuration $\bar{\mathcal{B}}$. The radial and circumferential stretches of the map from the reference configuration to $\bar{\mathcal{B}}$ are

$$\bar{\lambda}_1 = \frac{d\bar{r}}{dR}, \qquad \bar{\lambda}_2 = \frac{\bar{r}}{R}, \qquad \bar{J} = \bar{\lambda}_1 \bar{\lambda}_2^2 > 0. \tag{74}$$

Both stretches are positive. For a spherical incremental growth motion the associated rate tensor has the form

$$\bar{L} = \operatorname{diag}(\bar{L}_{11}, \bar{L}_{22}, \bar{L}_{22}), \qquad \bar{L}_{11} = \frac{\partial_t \bar{\lambda}_1}{\bar{\lambda}_1}, \quad \bar{L}_{22} = \frac{\partial_t \bar{\lambda}_2}{\bar{\lambda}_2} = \frac{\partial_t \bar{r}}{\bar{r}}. \tag{75}$$

Here ∂_t denotes evolution at a fixed physical growth instant; the prime used below denotes differentiation in the *spatial* variable R. These two derivatives must not be confused.

Let $\tau = \operatorname{diag}(\tau_1, \tau_2, \tau_2)$ denote a residual-stress field in the intermediate description. Its increments $\delta\tau_1$ and $\delta\tau_2$ are the radial and circumferential stress increments, respectively, and need not equal the current Cauchy traction. The spatial state and scalar control are chosen as

$$y(R) = \begin{bmatrix} y_1(R) \\ y_2(R) \end{bmatrix} = \begin{bmatrix} \delta\tau_1(R) \\ \bar{L}_{22}(R) \end{bmatrix}, \qquad u(R) = \delta\tau_2(R). \tag{76}$$

The state components therefore combine a stress increment with a radial profile of circumferential growth rate; the control is a second stress increment. In numerical examples the fields are nondimensionalized by fixed stress and rate scales.

The incremental radial equilibrium relation and a radial compatibility/constitutive relation have the scalar form

$$\frac{dy_1}{dR} = -2\chi(R)\,[y_1 - u], \tag{77}$$

$$\frac{dy_2}{dR} = \frac{\chi(R)}{\gamma_{01}(R)}\big[y_1 - u + (\gamma_{02}(R) - \gamma_{01}(R))y_2\big]. \tag{78}$$

Here $\chi(R) = \bar{\lambda}_1/(R\bar{\lambda}_2)$ is the geometry factor and γ_{01}, γ_{02} are incremental stress–growth moduli. For the stress-dependent quadratic elastic law used as one possible specialization in Huang [15], these moduli take the form

$$\gamma_{0i} = \bar{J}^{-1}\bar{\lambda}_i^2(\mu_{\mathrm{e}} + \tau_{0i}) + \bar{p}, \qquad i = 1, 2, \tag{79}$$

where μ_{e} is a shear modulus, τ_{0i} are principal reference residual-stress components, and $\bar{p}$ is the pressure-like multiplier associated with incompressibility. Our analysis requires only $\gamma_{01} \neq 0$ and prescribed coefficients; other constitutive models may provide different effective moduli. At each fixed growth step, the stretches and moduli are evaluated from the *pre-incremental* shell and treated as functions of R, not as unknowns evolving with the spatial ODE.

The corresponding state equation, obtained directly from the two scalar relations above, is

$$y' = A_{\mathrm{phys}}(R)y + B_{\mathrm{phys}}(R)u, \tag{80}$$

with

$$A_{\mathrm{phys}}(R) = \chi(R)\begin{bmatrix} -2 & 0 \\ \gamma_{01}^{-1} & (\gamma_{02}-\gamma_{01})/\gamma_{01} \end{bmatrix}, \tag{81}$$

$$B_{\mathrm{phys}}(R) = \chi(R)\begin{bmatrix} 2 \\ -\gamma_{01}^{-1} \end{bmatrix}. \tag{82}$$

Notice that the physical state reduction does not by itself close a *time-dependent* growth law. It is one incremental spatial step, supplied with its initial state, constitutive coefficients and objective functional.

Incremental radial traction-free conditions on the intermediate shell give $\delta\tau_1(R_i) = \delta\tau_1(R_o) = 0$. The initial circumferential rate is prescribed by coupling to the inner-surface growth step, say $\bar{L}_{22}(R_i) = \ell_i$. Thus

$$y(R_i) = \begin{bmatrix} 0 \\ \ell_i \end{bmatrix}, \qquad y_1(R_o) = 0, \qquad y_2(R_o) \text{ not prescribed.} \tag{83}$$

This is a mixed mechanical endpoint even though the terminal cost may penalize both components. For the quadratic terminal cost

$$\Phi(y(R_o)) = \tfrac{1}{2}(y(R_o) - r_o)^T H(y(R_o) - r_o), \tag{84}$$

where $r_o \in \mathbb{R}^2$ is the preferred terminal state and $H = H^T \succeq 0$ is its weight, the costate condition is

$$p(R_o) = H(y(R_o) - r_o) + \nu e_1, \qquad e_1 = (1,0)^T. \tag{85}$$

The free second component imposes $p_2(R_o) = [H(y(R_o) - r_o)]_2$; the first costate component is determined through the multiplier ν and the remote traction condition. Standard affine Riccati terminal data for K and z remain valid if the additional term $Z\nu$ is retained.

6.2 A mechanically derived closed-form shell calculation

For a transparent physical reduction take the *frozen* dimensionless coefficients

$$R_i = 1, \quad R_o = 2, \quad \bar{\lambda}_1/\bar{\lambda}_2 = 1, \quad \gamma_{01} = \gamma_{02} = 1. \tag{86}$$

Equations (77)–(78) reduce exactly to

$$y' = \frac{1}{R}\begin{bmatrix} -2 & 0 \\ 1 & 0 \end{bmatrix} y + \frac{1}{R}\begin{bmatrix} 2 \\ -1 \end{bmatrix} u. \tag{87}$$

Choose $y(1) = (0,1)^T$, impose the outer traction condition $y_1(2) = 0$, and minimize

$$\mathcal{J} = \frac{1}{2} y_2(2)^2 + \frac{1}{2}\int_1^2 [u(R) - 1]^2 \, dR. \tag{88}$$

The reference value $u_0 = 1$ is a nonzero preferred circumferential stress increment. From (87), $y_2' = -\frac{1}{2}y_1'$, so $y_2(R) = 1 - y_1(R)/2$. In particular, $y_2(2) = 1$ for every mechanically admissible control satisfying $y_1(2) = 0$. Furthermore

$$\frac{d}{dR}\left(R^2 y_1\right) = 2Ru, \quad \text{so} \quad \int_1^2 Ru(R)\, dR = 0 \tag{89}$$

expresses the terminal traction exactly. Minimizing the remaining quadratic cost subject to this linear integral condition gives

$$u_{\mathrm{con}}(R) = 1 - \frac{9}{14}R, \tag{90}$$

$$y_{1,\mathrm{con}}(R) = \frac{7R^2 - 3R^3 - 4}{7R^2}, \tag{91}$$

$$y_{2,\mathrm{con}}(R) = 1 - \frac{1}{2} y_{1,\mathrm{con}}(R). \tag{92}$$

The costate equations yield $p_2 = \alpha$, $p_1 = \beta R^2 + \alpha/2$, and $u = 1 - 2\beta R$. Thus $\alpha = 1$, $\beta = 9/28$ and

$$\nu = p_1(2) = \frac{25}{14} \neq 0. \tag{93}$$

If the mechanical terminal condition is instead replaced by $p_1(2) = 0$, the free-endpoint solution has $p_2 = 6/11$ and

$$u_{\mathrm{free}}(R) = 1 + \frac{3R}{22}, \quad y_{1,\mathrm{free}}(2) = \frac{10}{11} \neq 0, \quad y_{2,\mathrm{free}}(2) = \frac{6}{11}. \tag{94}$$

Both controls solve the same spatial shell equations and start from the same mechanical state; only the treatment of the external traction condition differs. The free-endpoint solution violates $y_1(2) = 0$ by the exact amount $10/11$. Figure 1 displays the resulting stress and adjoint trajectories. In particular, the multiplier changes the entire stress distribution, not only the terminal costate value.

The two panels in Fig. 1 show how a condition imposed at the external material boundary changes the entire spatial control field. Both solutions share the same dynamics, cost and initial data. The finite terminal stress residual results solely from substituting free-endpoint transversality for the prescribed mechanical boundary

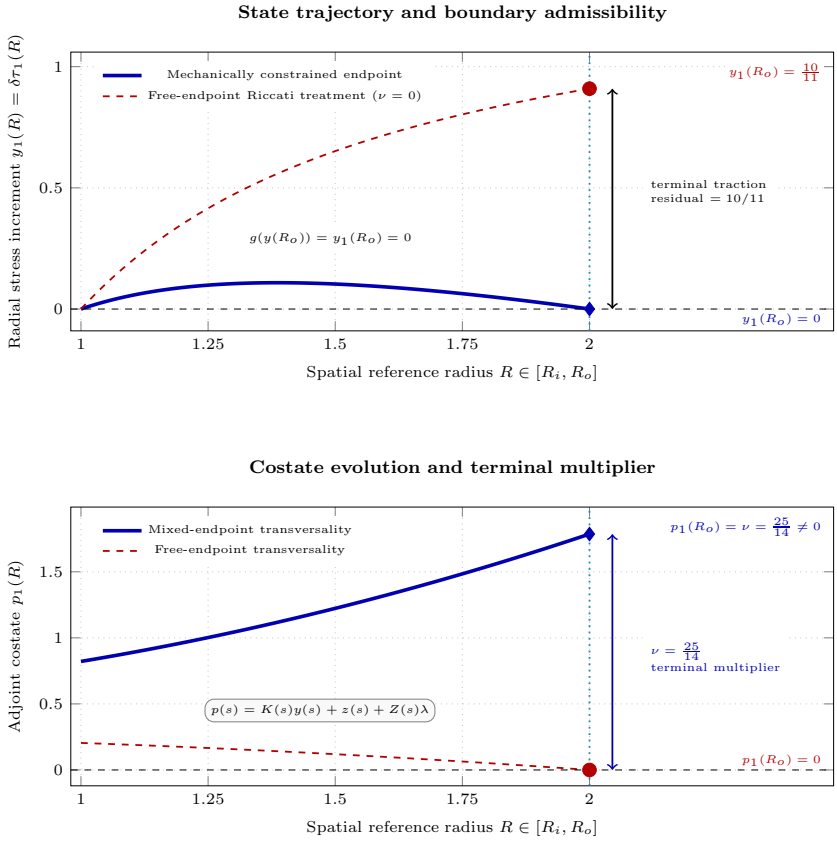

Fig. 1 Exact effect of terminal mechanical admissibility on the radial shell regulator (87)–(88). Top: the constrained stress increment (blue) satisfies $y_1(2) = 0$, while the free-endpoint solution (red) terminates at $y_1(2) = 10/11$. Bottom: the corresponding costate fields; the constrained solution has terminal multiplier $\nu = p_1(2) = 25/14$, whereas the free-endpoint solution satisfies $p_1(2) = 0$. Both trajectories use the same shell equations and initial state $y(1) = (0, 1)^T$.

condition. The nonzero endpoint multiplier is the dual response that restores the admissible radial-stress boundary value.

6.3 A two-state shell test with unequal incremental moduli

The preceding closed-form benchmark admits the special identity $y_2 = 1 - y_1/2$. This identity is not needed by the endpoint method. To verify the fully two-state calculation, retain $\chi = 1/R$ and $\gamma_{01} = 1$ but set $\gamma_{02} = 2$ at the same fixed growth step. The shell equations then become

$$y' = \frac{1}{R}\begin{bmatrix} -2 & 0 \\ 1 & 1 \end{bmatrix} y + \frac{1}{R}\begin{bmatrix} 2 \\ -1 \end{bmatrix} u, \qquad y(1) = (0, 1)^T, \tag{95}$$

with the identical objective (88) and the outer radial-stress condition $y_1(2) = 0$. The second state now has its own spatial evolution, so the control problem retains the full two-dimensional state structure. The unequal-modulus choice is a frozen-coefficient shell benchmark; its realization in a specific constitutive material requires compatible pre-incremental stress and deformation fields.

The transition matrix of the homogeneous system is $(R/t)^M$, $M = \left[\begin{smallmatrix} -2 & 0 \\ 1 & 1 \end{smallmatrix}\right]$. At $R = 2$, write

$$y_1(2) = \int_1^2 h(t)u(t)\,dt, \qquad y_2(2) = 2 + \int_1^2 k(t)u(t)\,dt, \tag{96}$$

where

$$h(t) = \frac{t}{2}, \qquad k(t) = -\frac{2}{3t^2} - \frac{t}{6}. \tag{97}$$

The constrained stationary control consequently has the explicit form

$$u_{\mathrm{con}}(t) = 1 - a\,k(t) - \nu h(t), \qquad a = y_2(2), \quad \nu = p_1(2). \tag{98}$$

Let $H_0 = \int_1^2 h\,dt$, $H_2 = \int_1^2 h^2\,dt$, $K_0 = \int_1^2 k\,dt$, $K_2 = \int_1^2 k^2\,dt$ and $K_H = \int_1^2 kh\,dt$. Direct integration gives

$$\begin{gathered} H_0 = \frac{3}{4}, \quad H_2 = \frac{7}{12}, \quad K_0 = -\frac{7}{12}, \\ K_2 = \frac{7}{36} + \frac{2\log 2}{9}, \qquad K_H = -\frac{7}{36} - \frac{\log 2}{3}. \end{gathered} \tag{99}$$

The terminal equality and the terminal costate condition give

$$\begin{bmatrix} 1 + K_2 & K_H \\ K_H & H_2 \end{bmatrix} \begin{bmatrix} a \\ \nu \end{bmatrix} = \begin{bmatrix} 2 + K_0 \\ H_0 \end{bmatrix}. \tag{100}$$

This matrix is positive definite: its quadratic form equals $a^2 + \int_1^2 (ak + \nu h)^2\,dt$ and can vanish only for $a = \nu = 0$. Thus the solution is unique. It gives

$$y_{2,\mathrm{con}}(2) = 1.8916306762, \qquad \nu_{\mathrm{con}} = 2.6655026844, \qquad y_{1,\mathrm{con}}(2) = 0. \tag{101}$$

Without the terminal mechanical equality, the same problem has $\nu = 0$, $a = (2 + K_0)/(1 + K_2)$ and hence

$$y_{1,\mathrm{free}}(2) = 1.1970097727, \qquad y_{2,\mathrm{free}}(2) = 1.0505677945. \tag{102}$$

The unequal-modulus calculation demonstrates the same terminal multiplier mechanism in the two-state shell equations without relying on the special invariant of the preceding example. The propagation formula $Z\lambda$ in Section 3 gives the corresponding Riccati implementation for general prescribed coefficient functions.

6.4 Mass supply and a source-dependent growth constraint

The reference density in the unloaded formulation is $\rho_0 = \bar{\rho}\bar{J}$, where $\bar{\rho}$ is mass per intermediate volume. If $\bar{\rho}$ is independent of time, elastic volume preservation gives $\rho = \bar{\rho}$ and, by differentiating $\bar{J}$,

$$\dot{\rho}_0 = \rho_0 \operatorname{tr} \bar{L}, \qquad \Gamma = \rho \operatorname{tr} \bar{L}. \tag{103}$$

The stress–growth relation underlying (78) provides

$$\bar{L}_{11} = \frac{\gamma_{02} y_2 + y_1 - u}{\gamma_{01}}, \tag{104}$$

so that

$$\operatorname{tr} \bar{L}(y, u, R) = \frac{y_1}{\gamma_{01}} + \left(2 + \frac{\gamma_{02}}{\gamma_{01}}\right) y_2 - \frac{u}{\gamma_{01}}. \tag{105}$$

Here the growth-rate trace is obtained from the same mechanical variables used in the spatial state equation; no density derivative has been added ad hoc. With $\Delta\psi_s := \psi_s - \psi$ and $\rho > 0$ constant in the unloaded-density idealization, the source contribution to the local isothermal dissipation is

$$\mathcal{D}_{\mathrm{src}} = \rho \Delta\psi_s \operatorname{tr} \bar{L}. \tag{106}$$

The mechanical part $\mathcal{D}_{\mathrm{mech}} = \sigma : D - \rho\dot{\psi}$ is fixed only after the stored energy and the other constitutive kinetics are specified. At a frozen growth step, an independently specified reduced affine response can be written as

$$\mathcal{D}_{\mathrm{mech}} = d_0(R) + d_1(R) y_1 + d_2(R) y_2 + d_u(R) u. \tag{107}$$

For a given constitutive law, the d_i are determined by its local stress-power and free-energy derivatives; they are not fixed by radial equilibrium alone. Inserting (105) into the full dissipation gives

$$\mathcal{D}_s = \mathcal{D}_{\mathrm{mech}} + \rho \Delta\psi_s \operatorname{tr} \bar{L}(y, u, R) \geq 0, \qquad \Delta\psi_s := \psi_s - \psi. \tag{108}$$

At fixed R with prescribed ρ and $\Delta\psi_s = \Delta$, the effective affine coefficients of (y_1, y_2, u) are

$$\begin{aligned} d_1^{\mathrm{eff}} &= d_1 + \frac{\rho\Delta}{\gamma_{01}}, \\ d_2^{\mathrm{eff}} &= d_2 + \rho\Delta\left(2 + \frac{\gamma_{02}}{\gamma_{01}}\right), \\ d_u^{\mathrm{eff}} &= d_u - \frac{\rho\Delta}{\gamma_{01}}. \end{aligned} \tag{109}$$

In particular, $d_1^{\mathrm{eff}} + d_u^{\mathrm{eff}} = d_1 + d_u$: source energetics shifts the admissibility half-space in a constrained direction, but does not erase constitutive compatibility relations between its mechanical coefficients.

Such compatibility is material-dependent. As a concrete check, in the incompressible quadratic residual-stress specialization discussed by Huang [15], elimination of $\bar{L}_{11}$ gives coefficients of y_1 and u of the form

$$d_1 = A_e - \frac{1}{2}(\lambda_e^{-4} - 1), \qquad d_u = -A_e - (\lambda_e^2 - 1), \tag{110}$$

where $\lambda_e > 0$ is the elastic circumferential stretch and A_e groups the common stress/modulus term. Hence

$$d_1 + d_u = \frac{3}{2} - \lambda_e^2 - \frac{1}{2}\lambda_e^{-4} \leq 0, \tag{111}$$

with equality at $\lambda_e = 1$; the inequality follows by minimizing $t + 1/(2t^2)$ for $t = \lambda_e^2 > 0$. The identity (111) provides a constitutive compatibility criterion for transferring reduced dissipation coefficients between material models.

The active-set calculation below employs the prescribed dimensionless affine reduced-dissipation law $\mathcal{D}_{\text{mech}} = y_2 + u$, whose coefficients constitute independent model data. The resulting control problem couples this closure with the shell equilibrium and compatibility equations, permitting an exact analysis of source-dependent admissibility and optimal switching. A constitutive realization in a particular hyperelastic material requires its own compatible free-energy and kinetic specification.

6.5 Activation of the dissipation constraint and the optimal switching arc

We now solve a coupled endpoint- and path-constrained growth-control problem using the shell equations (87). Set $R \in [1, 2]$, $y(1) = (0, 1)^T$, and prescribe the terminal radial-stress increment $y_1(2) = 0$. The cost remains (88). To isolate the effect of supplied-mass energetics within the reduced class (107), prescribe the dimensionless affine response

$$\mathcal{D}_{\text{mech}} = y_2 + u, \qquad \rho = 1, \qquad \Delta := \psi_s - \psi \in \{0, -3/10\}. \tag{112}$$

The addition in $y_2 + u$ is meaningful after nondimensionalization by the stress-power and rate scales of this reduced model. The source energy ψ_s is specified relative to the local free energy so that Δ is held constant during this frozen incremental solve. These choices define a phenomenological affine reduced-dissipation benchmark; they do not identify its coefficients with those of (110). The growth-rate trace is $\operatorname{tr} \bar{L} = y_1 + 3y_2 - u$ by (105). Thus the local thermodynamic restriction reads

$$\mathcal{D}_s = y_2 + u + \Delta(y_1 + 3y_2 - u) \geq 0, \tag{113}$$

and is imposed at every material radius. Since $\partial_u \mathcal{D}_s = 1 - \Delta > 0$, it is a regular mixed state–control constraint.

A useful simplification follows directly from the two shell state equations. Writing $x(R) = y_1(R)$, we have

$$y_2(R) = 1 - \frac{x(R)}{2}, \qquad x'(R) = \frac{2}{R}\big(u(R) - x(R)\big), \qquad x(1) = x(2) = 0. \tag{114}$$

The terminal cost $y_2(2)^2/2 = 1/2$ is consequently fixed by mechanical admissibility. Minimization therefore reduces to $\frac{1}{2}\int_1^2 (u-1)^2\, dR$ under the scalar state equation and the dissipation inequality

$$\mathcal{D}_s = (1 + 3\Delta) - \frac{1+\Delta}{2}x + (1-\Delta)u \geq 0. \tag{115}$$

For $\Delta < 1$ this is the explicit unilateral control bound

$$u(R) \geq \frac{\frac{1}{2}(1+\Delta)x(R) - (1+3\Delta)}{1-\Delta}. \tag{116}$$

The mechanics and the second law thus determine a convex feasible set in the same spatial control variable.

Exact threshold for activation.

The mechanically constrained, source-neutral solution (90)–(91) has

$$\mathcal{D}_{\mathrm{mech}}(R) = \frac{3}{2} - \frac{3R}{7} + \frac{2}{7R^2}, \tag{117}$$

$$\operatorname{tr}\bar{L}(R) = \frac{3}{2} + \frac{6R}{7} + \frac{2}{7R^2}. \tag{118}$$

Define $A(R) = \mathcal{D}_{\mathrm{mech}}(R)$ and $B(R) = \operatorname{tr}\bar{L}(R)$ for this source-neutral control, with the explicit positive functions given in (117)–(118). Then $\mathcal{D}_s = A + \Delta B$. The quotient satisfies

$$\frac{d}{dR}\frac{A(R)}{B(R)} = -\frac{54R^2(7R^2+4)}{(12R^3+21R^2+4)^2} < 0 \quad (1 \leq R \leq 2). \tag{119}$$

Since $A, B > 0$ and $A(2)/B(2) = 5/23$, the previously optimal mechanically admissible control satisfies the dissipation inequality at *every* radius if and only if

$$\Delta \geq \Delta_c := -\frac{5}{23}. \tag{120}$$

This threshold characterization holds for all real Δ within the prescribed affine model. In the range $-3/10 \leq \Delta \leq 0$, the dissipation itself is strictly decreasing in R, with

$$\min_{R\in[1,2]} \mathcal{D}_s(R) = \mathcal{D}_s(2) = \frac{5+23\Delta}{7}. \tag{121}$$

In particular, $\Delta = 0$ produces a strictly positive dissipation margin, with minimum $5/7$, and optimal cost $\mathcal{J}_0 = 55/56$. For $\Delta = -3/10 < \Delta_c$, the same control gives $\mathcal{D}_s(2) = -19/70$. The source-energy closure therefore changes the admissible set and requires a new optimum.

Closed-form active arc.

At $\Delta = -3/10$, Eq. (115) becomes

$$\mathcal{D}_s = \frac{2 - 7x + 26u}{20} \geq 0, \qquad u \geq \frac{7x - 2}{26}. \tag{122}$$

We construct a one-switch candidate with an inactive interval $[1, R_*)$ and an active interval $[R_*, 2]$, and subsequently certify that it is the unique global optimum. On the inactive interval the standard stationarity equation with the terminal mechanical constraint gives, for a constant β,

$$u_-(R) = 1 - 2\beta R, \tag{123}$$

$$x_-(R) = 1 - \frac{4\beta R}{3} + \frac{4\beta/3 - 1}{R^2}. \tag{124}$$

On the active interval, the thermodynamic boundary $\mathcal{D}_s = 0$ fixes $u = (7x - 2)/26$. Substitution in the mechanical equation yields

$$Rx' = -\frac{19x + 2}{13}, \qquad x(2) = 0, \tag{125}$$

with the exact solution

$$x_+(R) = \frac{2}{19}\left[\left(\frac{2}{R}\right)^{19/13} - 1\right], \tag{126}$$

$$u_+(R) = \frac{7x_+(R) - 2}{26}. \tag{127}$$

Continuity of the mechanical state and the optimal control determines (β, R_*) from

$$x_-(R_*) = x_+(R_*), \qquad 1 - 2\beta R_* = \frac{7x_+(R_*) - 2}{26}. \tag{128}$$

Solving these two scalar equations gives

$$R_* = 1.4927095693, \qquad \beta = 0.3556627869. \tag{129}$$

The resulting continuous optimal cost is

$$\begin{aligned}\mathcal{J}_* &= \frac{1}{2} + \frac{1}{2}\int_1^{R_*} (u_- - 1)^2\, dR + \frac{1}{2}\int_{R_*}^{2} (u_+ - 1)^2\, dR \\ &= 0.9867032001.\end{aligned} \tag{130}$$

Continuous optimality certificate.

The constructed active-arc solution satisfies the mixed-constraint Pontryagin conditions. We establish a global optimality and uniqueness certificate for the resulting constrained control problem. For the reduced problem (114), the augmented Hamiltonian is

$$\mathcal{H}_a = \frac{1}{2}(u-1)^2 + \frac{2p}{R}(u - x) - \mu\,\frac{2 - 7x + 26u}{20}. \tag{131}$$

Stationarity and the adjoint equation read

$$u - 1 + \frac{2p}{R} - \frac{13}{10}\mu = 0, \qquad p' = \frac{2p}{R} - \frac{7}{20}\mu. \tag{132}$$

On the inactive arc, set $\mu = 0$ and $p = \beta R^2$; these equations give (123). On the active arc, let

$$p = \frac{R}{2}\left(1 - u_+ + \frac{13}{10}\mu\right), \qquad \mu(R_*) = 0. \tag{133}$$

Equations (132) then reduce to

$$\frac{13}{10}R\mu' - \frac{3}{5}\mu = 1 - u_+ + Ru_+' = \frac{175 - 112x_+}{169} > 0 \quad (R_* \le R \le 2). \tag{134}$$

Because $0 \le x_+(R) \le x_+(R_*) < 2/19$, the forcing on the right of (134) is strictly positive. Multiplication by the positive integrating factor $R^{-6/13}$ and integration from R_* proves $\mu(R) > 0$ on $(R_*, 2]$. On the inactive interval the dissipation decreases strictly, as

$$\mathcal{D}_s'(R) = -\frac{64\beta R^3 - 28\beta + 21}{30R^3} < 0 \qquad (1 \le R < R_*), \tag{135}$$

and $\mathcal{D}_s(R_*) = 0$; hence $\mathcal{D}_s > 0$ before the switch. The state and costate are continuous at R_*, the control is continuous by (128), and all state, endpoint, stationarity and complementary-slackness conditions hold.

A direct cost-difference calculation now establishes sufficiency without appealing only to a general convexity assertion. Let $\widetilde{u}$ be any other feasible control, with associated state $\widetilde{x}$, and set $\delta u = \widetilde{u} - u_*$, $\delta x = \widetilde{x} - x_*$. Both states obey $x(1) = x(2) = 0$, so the terminal cost $y_2(2)^2/2 = 1/2$ cancels. Expanding the running cost and using

stationarity gives

$$\begin{aligned}\mathcal{J}[\widetilde{u}] - \mathcal{J}[u_*] &= \frac{1}{2}\int_1^2 (\delta u)^2\, dR + \int_1^2 (u_* - 1)\delta u\, dR \\ &= \frac{1}{2}\int_1^2 (\delta u)^2\, dR + \int_1^2 \mu(R)\left[\mathcal{D}_s(\widetilde{x},\widetilde{u}) - \mathcal{D}_s(x_*,u_*)\right] dR.\end{aligned} \tag{136}$$

For the second identity substitute $u_* - 1 = -2p/R + (13/10)\mu$, use $\delta x' = (2/R)(\delta u - \delta x)$, integrate the costate term by parts, and invoke $p' = 2p/R - (7/20)\mu$. The endpoint term vanishes because $\delta x(1) = \delta x(2) = 0$. The remaining linear terms combine into $\mu\,\delta\mathcal{D}_s$ because $\delta\mathcal{D}_s = (-7\delta x + 26\delta u)/20$.

Since $\mathcal{D}_s(\widetilde{x},\widetilde{u}) \geq 0$, $\mu \geq 0$ and $\mu\mathcal{D}_s(x_*,u_*) = 0$, the second integral is nonnegative. Therefore

$$\mathcal{J}[\widetilde{u}] - \mathcal{J}[u_*] \geq \frac{1}{2}\|\widetilde{u} - u_*\|^2_{L^2(1,2)}, \tag{137}$$

with equality only for the same control almost everywhere. This proves global optimality, unique optimal control and unique associated state, and rules out any different optimal switching pattern. The multiplier at the outer boundary is nonzero as well: restoring the full costate gives $p_2(2) = y_2(2) = 1$ and $p_{\text{scalar}}(2) = p_1(2) - p_2(2)/2$, so

$$\mu(2) \simeq 0.2452305112, \qquad \nu_{\text{active}} = p_1(2) \simeq 1.8957227415. \tag{138}$$

Thus the continuous endpoint and active-path multipliers are simultaneously present in the exact constrained solution.

Independent numerical verification.

For computation, divide $[1,2]$ into N cells and hold u constant in each cell. The mechanical state can be propagated exactly across $[a,b]$:

$$y_1(b) = \left(\frac{a}{b}\right)^2 y_1(a) + \left[1 - \left(\frac{a}{b}\right)^2\right] u_j, \tag{139}$$

$$y_2(b) = y_2(a) - \frac{1}{2}[y_1(b) - y_1(a)]. \tag{140}$$

For constant u_j, the radial stress y_1 and the dissipation (115) are monotone within each cell. Consequently, imposing the linear inequality at both cell endpoints guarantees admissibility throughout the cell. The discretized cost is

$$\mathcal{J}_N = \frac{1}{2}y_2(2)^2 + \frac{1}{2N}\sum_{j=1}^{N}(u_j - 1)^2, \tag{141}$$

with the exact terminal condition $y_1(2) = 0$. This yields a finite-dimensional strictly convex quadratic program. The exact cell propagator and dissipation inequalities were implemented in Python, with additional admissibility checks at interior points of each cell. Table 1 confirms convergence to the two continuous optimal costs.

Table 1 Convergence of the cellwise-constant spatial optimization to the continuous mechanically and thermodynamically admissible solutions. The terminal radial-stress residual is below 10^{-14} for all reported computations.

	$\Delta = 0$		$\Delta = -0.30$	
N	$\mathcal{J}_N$	$y_2(2)$	$\mathcal{J}_N$	$y_2(2)$
40	0.98215362	1.00000000	0.98673755	1.00000000
80	0.98214555	1.00000000	0.98671855	1.00000000
160	0.98214353	1.00000000	0.98671043	1.00000000
Continuous	0.98214286	1	0.98670320	1

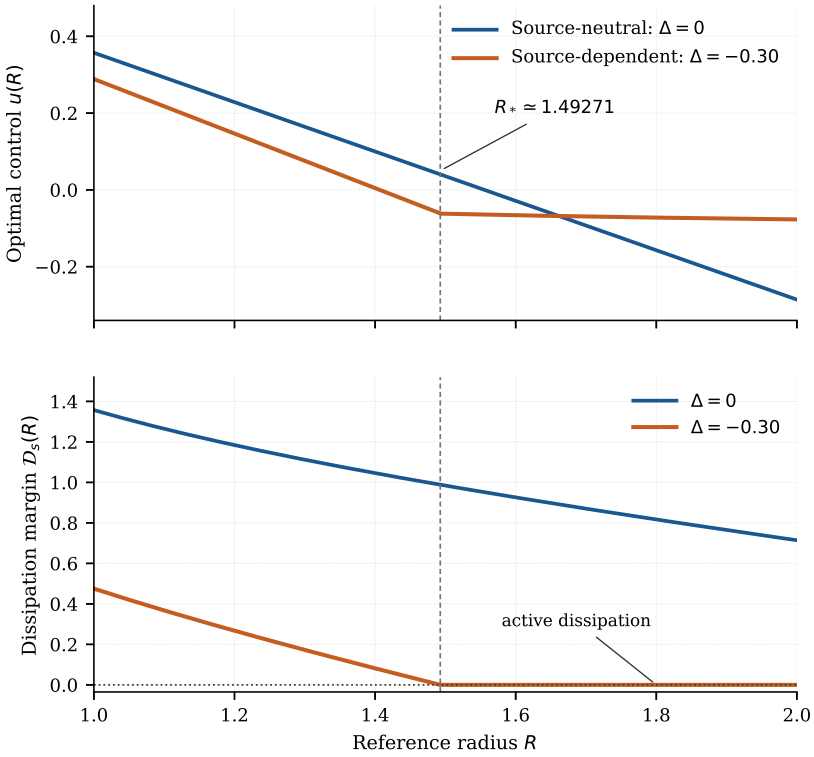

Fig. 2 Source-energy dependence of the optimal spatial control (upper panel) and the local dissipation margin (lower panel) for the reduced shell problem (87), (112). At $\Delta = 0$ the inequality is inactive. At $\Delta = -0.30$ the control enters the exactly determined active arc at $R_* = 1.49271$; the dissipation then reaches zero. Both profiles satisfy the prescribed radial-stress boundary conditions.

Figure 2 exhibits two distinct optimality mechanisms within a single spatial shell model. The endpoint condition determines the global stress-compatible control, while the source-energy closure determines whether that control is permitted along the radius. Below the activation threshold (120), the dissipation multiplier becomes positive on a finite interval and the control follows the thermodynamic boundary. In both solutions the growth-rate trace $\operatorname{tr} \bar{L} = 3 - x/2 - u$ is strictly positive, so the source term represents deposition of material. The explicit switching solution and the grid-refinement study jointly characterize the controlled response of this coupled endpoint/path-constrained model.

7 Mechanical and Thermodynamic Implications

The coupled formulation reveals two distinct but interacting mechanisms. The mechanical terminal manifold determines which radial stress profiles can be realized; the open-system dissipation inequality selects which of those profiles remain admissible under a specified mass-deposition energetics. In a linear-quadratic spatial reduction the mechanical constraint induces the propagated costate term $Z\lambda$. When the source-dependent dissipation becomes active, a second multiplier $\mu(R)$ modifies stationarity over a spatial interval. The resulting profile is determined jointly by endpoint matching, local thermodynamic admissibility, and convex optimality.

The exact terminal calculation in Fig. 1 isolates the mechanical issue. For the same reference shell equations, initial state and quadratic objective, the mechanically constrained solution gives $y_1(2) = 0$ with $\nu = 25/14$, while free-endpoint treatment gives $y_1(2) = 10/11$. The two-state unequal-modulus calculation in Section 6.3 provides an independent verification without the special scalar invariant; its nonzero multiplier similarly restores the external traction. The terminal mechanical equality is an essential boundary condition, independent of tracking penalties in the objective functional.

The source-energy analysis establishes an independent and complementary consequence. In the reference description the deposited-mass free-energy contribution takes the form $\psi_s \dot{\rho}_0$; in the intermediate unloaded description it appears as $\rho(\psi_s - \psi) \operatorname{tr} \bar{L}$. The source coefficient shift (109) makes its effect on the admissible half-space explicit. For the specified affine reduced-dissipation law, the source-neutral optimum remains feasible precisely for $\Delta \geq -5/23$. At $\Delta = -0.30$ the restriction creates an active arc $[1.49271, 2]$ with $\mathcal{D}_s = 0$, and the control follows the exact state-dependent bound (127). The cost-difference inequality (137) certifies global optimality and uniqueness. These results isolate the effect of deposition energetics on an optimal spatial growth-control field while keeping the constitutive closure explicit.

The analysis is carried out for a single-constituent, local-source growth model and one frozen radial increment. The shell equations follow from equilibrium and incremental compatibility; the affine dissipation law in the exact active-arc example is separately prescribed at reduced level. The coefficient check (111) demonstrates why constitutive coefficients must be identified with care before transferring this numerical benchmark to a particular hyperelastic solid. Repeated growth steps would require updating the geometry, moduli, residual stress and deposited-mass energetic variables. With additional constituents or relative mass fluxes, the mass, momentum

and entropy transports require a corresponding extension of the balance structure [3, 7]. In higher-dimensional spatial settings, equilibrium and compatibility produce coupled PDE constraints. The endpoint and dissipation mechanisms identified here supply the constraints that such extensions must retain.

8 Conclusions

A spatial growth-control solution must enforce terminal mechanical boundary data and local open-system dissipation jointly. We have derived a common control formulation with a propagated endpoint multiplier $Z\lambda$ and the source-energy contribution $\rho(\psi_s - \psi)\,\mathrm{tr}\,\bar{L}$. The mechanically derived shell equations give a closed-form boundary mismatch $y_1(2) = 10/11$ under free-endpoint treatment and the corresponding nonzero terminal multiplier $\nu = 25/14$; an unequal-modulus two-state test confirms the endpoint mechanism. For an explicitly prescribed affine reduced-dissipation law, the same shell reduction yields the exact activation threshold $\Delta_c = -5/23$, a continuous active-arc solution, the switching radius $R_* = 1.4927095693$, and a direct global optimality and uniqueness certificate. Constitutive compatibility conditions distinguish the generic source correction from any particular hyperelastic specialization. The resulting analysis supplies a transparent and reproducible framework for spatial optimization subject to both boundary and thermodynamic admissibility.

Appendix A A minimal mixed-endpoint control calculation

The distinction can be seen without any growth mechanics.

Let $s \in [0,1]$, $y = (y_1, y_2)^T$, $u = (u_1, u_2)^T$, and

$$y' = u, \qquad y(0) = \begin{bmatrix} a \\ b \end{bmatrix}. \tag{A1}$$

Minimize

$$\mathcal{J} = \frac{1}{2} h y_2(1)^2 + \frac{1}{2}\int_0^1 (u_1^2 + u_2^2)\, ds, \qquad h > 0, \tag{A2}$$

subject to the mechanical terminal condition

$$y_1(1) = 0, \qquad y_2(1) \text{ free.} \tag{A3}$$

The Hamiltonian is $\mathcal{H} = (u_1^2 + u_2^2)/2 + p^T u$, so $u = -p$ and $p' = 0$. The first terminal condition in (A3) gives

$$p_1(s) = a, \qquad u_1(s) = -a, \qquad y_1(s) = a(1-s). \tag{A4}$$

For the free second component,

$$p_2(1) = h y_2(1), \tag{A5}$$

which yields

$$p_2(s) = \frac{hb}{1+h}, \qquad y_2(1) = \frac{b}{1+h}. \tag{A6}$$

If the free-terminal condition $p_1(1) = \partial\Phi/\partial y_1 = 0$ were imposed in addition to $y_1(1) = 0$, then (A4) would require $a = 0$. Hence, for generic initial data, the free-terminal transversality condition is incompatible with the prescribed terminal mechanical state.

The example isolates the mechanism that appears in spatial mechanics: a prescribed endpoint stress or displacement component removes the corresponding endpoint variation and therefore removes the associated free-endpoint costate condition.

Statements and Declarations

Author contributions. RV: Conceptualization, methodology, formal analysis, and writing of the original draft.

Funding. The author declares that no financial support was received for the research presented in this article.

Data and code availability. No datasets were generated or analyzed during the current study. All analytical formulae and benchmark parameters are provided in the manuscript. The Python code used for exact cellwise state propagation, constrained spatial optimization and verification of the two-state shell benchmark is available from the author upon reasonable request.

Competing interests. The author declares no conflict of interest.

References

[1] M. Epstein, G. Maugin, Thermomechanics of volumetric growth in uniform bodies, Int. J. Plast. 16 (2000) 951–978. doi:10.1016/S0749-6419(99)00081-9.

[2] J. Humphrey, K. Rajagopal, A constrained mixture model for growth and remodeling of soft tissues, Math. Models Methods Appl. Sci. 12 (2002) 407–430. doi:10.1142/S0218202502001714.

[3] K. Garikipati, E.M. Arruda, K. Grosh, H. Narayanan, S. Calve, A continuum treatment of growth in biological tissue: The coupling of mass transport and mechanics, J. Mech. Phys. Solids 52 (2004) 1595–1625. doi:10.1016/j.jmps.2004.01.004.

[4] D. Ambrosi, G. Ateshian, E. Arruda, S. Cowin, J. Dumais, A. Goriely, G. Holzapfel, J. Humphrey, R. Kemkemer, E. Kuhl, J. Olberding, L. Taber, K. Garikipati, Perspectives on biological growth and remodeling, J. Mech. Phys. Solids 59 (2011) 863–883. doi:10.1016/j.jmps.2010.12.011.

[5] A. Menzel, E. Kuhl, Frontiers in growth and remodeling, Mech. Res. Commun. 42 (2012) 1–14. doi:10.1016/j.mechrescom.2012.02.007.

[6] A. Goriely, The Mathematics and Mechanics of Biological Growth, Springer, New York, 2017. doi:10.1007/978-0-387-87710-5.

[7] G.A. Ateshian, B.K. Zimmerman, Continuum thermodynamics of constrained reactive mixtures, J. Biomech. Eng. 144 (2022) 041011. doi:10.1115/1.4053084.

[8] N.M. Castoldi, P. Pivonka, L. Teresi, V. Sansalone, Modelling and simulation of growth driven by mechanical and non-mechanical stimuli, J. Mech. Phys. Solids 191 (2024) 105769. doi:10.1016/j.jmps.2024.105769.

[9] A. Erlich, G. Zurlo, Incompatibility-driven growth and size control during development, J. Mech. Phys. Solids 188 (2024) 105660. doi:10.1016/j.jmps.2024.105660.

[10] A. Grillo, A. Pastore, S. Di Stefano, An approach to growth mechanics based on the analytical mechanics of nonholonomic systems, J. Elasticity 157 (2025) 3. doi:10.1007/s10659-024-10092-7.

[11] T. Lekszycki, Functional adaptation of bone as an optimal control problem, J. Theor. Appl. Mech. 43 (2005) 555–574.

[12] U. Andreaus, M. Colloca, D. Iacoviello, An optimal control procedure for bone adaptation under mechanical stimulus, Control Eng. Pract. 20 (2012) 575–583. doi:10.1016/j.conengprac.2012.02.002.

[13] G. Jones, L. Mahadevan, Optimal control of plates using incompatible strains, Nonlinearity 28 (2015) 3153–3174. doi:10.1088/0951-7715/28/9/3153.

[14] M. Liu, L. Liang, H. Dong, W. Sun, R. Gleason, Constructing growth evolution laws of arteries via reinforcement learning, J. Mech. Phys. Solids 168 (2022) 105044. doi:10.1016/j.jmps.2022.105044.

[15] R. Huang, Modelling growth of soft solid as optimal control of nonlocal material manifolds, J. Mech. Phys. Solids 215 (2026) 106699. doi:10.1016/j.jmps.2026.106699.

[16] R. Huang, R.W. Ogden, R. Penta, Modelling volumetric growth in soft solids via residual stress, J. Elasticity 157 (2025) 73. doi:10.1007/s10659-025-10164-2.

[17] P. Brunovský, J. Komorník, The matrix Riccati equation and the noncontrollable linear-quadratic problem with terminal constraints, SIAM J. Control Optim. 21 (1983) 280–288. doi:10.1137/0321016.

[18] A. Ferrante, G. Marro, L. Ntogramatzidis, A parametrization of the solutions of the finite-horizon LQ problem with general cost and boundary conditions, Automatica 41 (2005) 1359–1366. doi:10.1016/j.automatica.2005.01.018.

[19] R.B. Vinter, Optimal Control, Birkhäuser, Boston, 2000.

[20] E. Kuhl, P. Steinmann, Mass- and volume-specific views on thermodynamics for open systems, Proc. R. Soc. A 459 (2003) 2547–2568. doi:10.1098/rspa.2003.1119.

[21] M. Gurtin, E. Fried, L. Anand, The Mechanics and Thermodynamics of Continua, Cambridge University Press, Cambridge, 2010. doi:10.1017/CBO9780511762956.

[22] F.H. Clarke, M.R. de Pinho, Optimal control problems with mixed constraints, SIAM J. Control Optim. 48 (2010) 4500–4524. doi:10.1137/090757642.

[23] A. Boccia, M.D.R. de Pinho, R.B. Vinter, Optimal control problems with mixed and pure state constraints, SIAM J. Control Optim. 54 (2016) 3061–3083. doi:10.1137/15M1041845.